AGU PUBLICATIONS

Journal of Advances in Modeling Earth Systems

REGULAR ARTICLE

10.1002/2013MS000255

Key Points:
- It develops a new assimilation scheme for the earth modeling
- It is the first application of the SPKF on the realistic oceanic model
- It promotes the new assimilation method in the earth modeling

Correspondence to:
Y. Tang,
ytang@unbc.ca

Citation:
Y. Tang, Z. Deng, K. K. Manoj, and D. Chen (2014), A practical scheme of the sigma-point Kalman filter for high-dimensional systems, *J. Adv. Model. Earth Syst.*, *6*, 21–37, doi:10.1002/2013MS000255.

Received 13 AUG 2013
Accepted 16 DEC 2013
Accepted article online 20 DEC 2013
Published online 24 JAN 2014

A practical scheme of the sigma-point Kalman filter for high-dimensional systems

Youmin Tang[1,2], Ziwang Deng[2,3], K. K. Manoj[2], and Dake Chen[1]

[1]State Key Laboratory of Satellite Ocean Environment Dynamics, Second Institute of Oceanography, State Oceanic Administration, Hangzhou, China, [2]Environmental Science and Engineering, University of Northern British Columbia, Prince George, British Columbia, Canada, [3]Department of Mathematics and Statistics, York University, Toronto, Ontario, Canada

Abstract While applying a sigma-point Kalman filter (SPKF) to a high-dimensional system such as the oceanic general circulation model (OGCM), a major challenge is to reduce its heavy burden of storage memory and costly computation. In this study, we propose a new scheme for SPKF to address these issues. First, a reduced rank SPKF was introduced on the high-dimensional model state space using the truncated single value decomposition (TSVD) method (T-SPKF). Second, the relationship of SVDs between the model state space and a low-dimensional ensemble space is used to construct sigma points on the ensemble space (ET-SPKF). As such, this new scheme greatly reduces the demand of memory storage and computational cost and makes the SPKF method applicable to high-dimensional systems. Two numerical models are used to test and validate the ET-SPKF algorithm. The first model is the 40-variable Lorenz model, which has been a test bed of new assimilation algorithms. The second model is a realistic OGCM for the assimilation of actual observations, including Argo and in situ observations over the Pacific Ocean. The experiments show that ET-SPKF is computationally feasible for high-dimensional systems and capable of precise analyses. In particular, for realistic oceanic assimilations, the ET-SPKF algorithm can significantly improve oceanic analysis and improve ENSO prediction. A comparison between the ET-SPKF algorithm and EnKF (ensemble Kalman filter) is also tribally conducted using the OGCM and actual observations.

1. Introduction

EnKF (ensemble Kalman filter)-based filters have gained great success in assimilating atmospheric and oceanic data [e.g., *Evensen*, 2003; *Zupanski*, 2005; *Tippett et al*., 2003; *Deng et al*., 2011]. However, concerns still exist, such as generating ensemble members and determining the ensemble size. The idea behind the EnKF algorithm is to "integrate" the Fokker-Plank equation using the ensemble technique to estimate the forecast error covariance. Theoretically, if the ensemble size is infinite, the estimation approaches the true value. In reality, however, only a finite ensemble size can be utilized, which inevitably leads to estimation errors. Thus, questions remain about the best method of determining the size of ensemble members given the accuracy of estimation and how directly the percentage of the estimated error variance is related to the true counterpart for a given ensemble size. The methods currently used for generating ensemble members in the standard EnKF [e.g., *Evesen*, 2003; *Tippett et al*., 2003] are generally unable to answer these questions. For example, the ensemble transform Kalman filters (ETKF) approach uses the analysis error covariance matrix to deterministically produce the ensemble, but it is incapable of measuring the estimation accuracy of up to the second-order moments related to the true values. In addition, the ETKF ensemble size is determined at the initial time and is randomly obtained.

Recently, a new ensemble-based filter that uses the simple Lorenz system, called the sigma-point Kalman filter (SPKF), was introduced to the field of earth science [e.g., *Ambandan and Tang*, 2009; *Luo and Moroz*, 2009]. The error statistics and state distributions for the SPKF method are calculated by the transformation of a deterministically chosen minimal set of weighted sample points called sigma points [*Julier et al*., 1995; *Julier and Uhlmann*, 2002; *Wan and der Merwe*, 2001; *Van der Merwe et al*., 2004]. For an L-dimensional system, represented by a set of discretized state space equations, the $2 * L + 1$ sigma points (i.e., ensemble members) constructed by the SPKF can precisely estimate the mean and covariance [*Julier et al*., 1995].

The important differences between the SPKF method and other Monte Carlo-based methods such as EnSRF (ensemble square root filter) and ETKF include the following: (1) random sampling (e.g., ensemble size) is

not used in SPKF, so the number of samples (ensemble member) required to approximate the mean and covariance is deterministic and relatively small [*Julier et al*., 1995]; (2) the accuracy of the SPKF method is at least up to the second-order moment (variance/covariance) for any nonlinearity and for random variables, and following a symmetric distribution, the estimation accuracy increases to the third order.

Despite being efficient among nonlinear filters and having widespread application in a variety of fields [e.g., *Fan and You*, 2009; *Van der Merwe and Wan*, 2001; *Van der Merwe et al*., 2004], the SPKF method is very costly when applied to atmospheric and oceanic systems because of their large dimensionality (L). There are a few schemes to reduce sigma points, such as the simplex SPKF [*Julier and Uhlmann*, 2002] and the marginal SPKF [*Morelande and Ristic*, 2006]. These methods can successfully reduce approximately 50% of the sigma points with the same order of accuracy as the traditional SPKF. However, the expense of these reduced SPKF methods is still computationally unfeasible for realistic atmospheric and oceanic models. *Ambadan and Tang* [2009] suggested the application of principle component analysis (PCA) for the error covariance matrix to select the most important sigma points that influence the evolution of error covariance. *Luo and Moroz* [2009] suggested the truncated singular value decomposition (TSVD) method to reduce sigma points (T-SPKF).

Further investigation is required for the application of SPKF on realistic high-dimensional models. First, the aforementioned reduced rank methods have thus far only been tested in the earth sciences with simple Lorenz models, and it is unclear whether these methods have acceptable estimation accuracy for high-dimensional, realistic atmospheric and oceanic models. Second, the reduced rank methods are based on an explicit expression of the prediction error covariance matrix, which usually exceeds the storage capacity of current computer systems [e.g., *Luo and Moroz*, 2009; *Ambadan and Tang*, 2009]. In EnKF-based filters, localization is a good strategy to overcome issues with storage; however, the sigma point in the SPKF method is determined based on the global domain, which makes it difficult to reduce the storage requirements.

In this study, we propose a new scheme to produce the sigma point, which uses the error covariance matrix on the ensemble space (called ET-SPKF). The scheme is first tested by the Lorenz 96 model and then further applied to an oceanic general circulation model (OCGM) for Argo data assimilation.

This paper is organized as follows: the SPKF algorithm is briefly described in section 2, the ET-SPKF method is developed in section 3, assimilation experiments to test and explore the ET-SPKF algorithm on 40-variable Lorenz 96 models are presented in section 4, the ET-SPKF algorithm is applied to a realistic OGCM for the assimilation of Argo and in site observations over the Pacific Ocean in section 5, and the discussion and comparisons between ET-SPKF and EnKF are in section 6.

2. SPKF Algorithm

The Kalman-based filters can estimate the model states using measurements described by the following:

$$\begin{aligned} x_t &= \psi(x_{t-1}, \eta_{t-1}) \qquad (\textit{dynamic}\ \text{model}) \\ y_t &= H(x_t, \varepsilon_t) \qquad (\textit{measurement}\ \text{model}) \end{aligned} \tag{1}$$

where x_t denotes the state variable, t denotes the time index, η_{t-1} denotes the dynamic process noise with the variance Q, ε_t denotes the measurement noise with the variance R, and y_t denotes the measurement. Functions ψ and H describe the evolution of the state variable over time and the relationship between the measurement and state, respectively.

The SPKF algorithm is similar to the EnKF algorithm, except it is based on a general formula of Kalman gain $K$and the analysis error covariance matrix P_a [e.g., *Ambadan and Tang*, 2009]:

$$\begin{aligned} K &= P_{\tilde{x}_b\tilde{y}} P_{\tilde{y}\tilde{y}}{}^{-1} \\ P_a &= P_{\tilde{x}_b\tilde{x}_b} - K P_{\tilde{x}_b\tilde{y}}, \end{aligned} \tag{2}$$

where $\tilde{x}^b$ is the forecast error and y is the observation error. These errors are defined by $\tilde{y}_t = \hat{y}_t - y_t$; $\tilde{x}_t^b = \hat{x}_t^b - x_t$, where $x_t{}^t$ and y_t are the true values at the time step of t for the model state and measurement and $\hat{x}_t^b$ and $\hat{y}_t$ are the corresponding prediction values:

$$\hat{x}^b{}_t = \psi(\hat{x}^a_{t-1})$$
$$\hat{y}_t = H(\hat{x}^b_t)$$

where $\hat{x}^a_{t-1}$ is the analysis value at the time step of $t-1$. Equation (2) can be interpreted as the cross-covariance $P_{\tilde{x}_b\tilde{y}}$ between the state and observation errors, and the remaining expression can be interpreted as the error covariance $P_{\tilde{y}\tilde{y}}$ of the difference between observation and its prediction $\hat{y}$. If measurement operator is linear or linearized (denoted by h) and noise is additive, i.e., $H = h, y_t = hx_t + \varepsilon_t, \hat{y}_t = h\hat{x}^b_t$, we arrive at the following:

$$\tilde{y}_t = \hat{y}_t - y_t = H(\hat{x}^b_t) - H(x_t, \varepsilon_t) = h\hat{x}^b_t - hx_t - \varepsilon_t$$
$$P_{\tilde{x}_b\tilde{y}} = E[(\hat{x}^b_t - x_t)(\hat{y}_t - y_t)^T] = E[\hat{x}^b_t - x_t][h(\hat{x}^b_t - x_t) - \varepsilon_t]^T = P_{\tilde{x}_b\tilde{x}_b}h^T$$
$$P_{\tilde{y}\tilde{y}} = E[(\hat{y}_t - y_t)(\hat{y}_{i,t} - y_t)^T] = E[(h\hat{x}^b_t - hx_t - \varepsilon_t)(h\hat{x}^b_t - hx_t - \varepsilon_t)^T] = hP_{\tilde{x}_b\tilde{x}_b}h^T + R$$

where $R = E(\varepsilon_t\varepsilon_t^T)$. Thus, the optimal Kalman gain was equal to the following:

$$K = P_{\tilde{x}_b\tilde{y}}P_{\tilde{y}\tilde{y}}{}^{-1} = P_{\tilde{x}_b\tilde{x}_b}h^T(hP_{\tilde{x}_b\tilde{x}_b}h^T + R)^{-1} \tag{3}$$

One of the primary differences between SPKF and EnKF is in the generation of ensembles. In SPKF, the ensemble members are produced deterministically by the sigma point, χ:

$$\begin{aligned}\chi_{t,0} &= \bar{X}^a_t;\\ \chi^+_{t,i} &= \bar{X}^a_t + [c\sqrt{P^a_X}]_{t,i}\\ \chi^-_{t,i} &= \bar{X}^a_t - [c\sqrt{P^a_X}]_{t,i}\end{aligned} \tag{4}$$

where the subscript t denotes time step, $\chi_t = [\chi_{t,0}, \chi^+_{t,i}, \chi^-_{t,i}]$, i = 1, 2, …, L; X is the augmented state vector, $X_t = [x_t, \eta_t, \varepsilon_t]$. $L = N_x + N_\eta + N_\varepsilon$ are the summed dimensions of model states (N_x), model noise (N_η) and measurement noise (N_ε). The scale parameter is c, which will be specified later. $[P^a_x]_i$ is the ith row (column) of the covariance matrix P^a_X (L * L dimension), defined by the following:

$$P^a_x = X^a_t \times (X^a_t)^{tr} \tag{5}$$

where the superscript "tr" denotes the transpose and the matrix product "×" is the external product in this manuscript (unless otherwise indicated). Equation (4) provides 2L + 1 sigma points χ_t, which are used as initial conditions to integrate model (1) and generate the ensemble members. The procedure is summarized below.

2.1. Initialization and Recursion

A small amount, denoted by $\Delta\zeta$, is perturbed on initial condition x_0 by a specific scheme, such as the *Evensen* [2003] method; and meanwhile randomly generates a perturbation for η and ε that is drawn from normal distributions of N(0, Q) and N(0, R). This is repeated M0 times.

The augmented state vector is denoted by $\Delta X = [\Delta\zeta, \eta, \varepsilon]$ and

$$\tilde{X}_0 = [\Delta X^1, \ldots, \Delta X^i, \ldots, \Delta X^{M0}]$$

where the superscript i is the number of perturbations. The analysis error covariance matrix of the initial step can be obtained by the following perturbation:

$$P^a_x = \tilde{X}_0\tilde{X}_0{}^{tr} \tag{6}$$

where X_0 is the matrix of L by M0 and P^a_x is a matrix of L by L.

From equation (6), we can calculate sigma points χ_t using equation (4) for model (1) to produce 2L+1 ensemble members. This calculation produces the analysis mean and covariance, which are used to produce sigma points to form a recursive algorithm.

2.2. Model Forecast

$$(\hat{x}^b_{t+1})_i = \psi(\chi_{t,i}) \tag{7}$$

$$\bar{\hat{x}}^b_{t+1} = \sum_i^{2L} w_i^{(m)} (\hat{x}^b_{t+1})_i \tag{8}$$

$$(\hat{y}_{t+1})_i = H(\hat{x}^b_{t+1,i}) \tag{9}$$

$$\bar{\hat{y}}_{t+1} = \sum_i^{2L} w_i^{(m)} (\hat{y}_{t+1})_i \tag{10}$$

$$(P_{\hat{x}^b,\hat{x}^b})_{t+1} = \sum_i^{2L} w_i^{(c)} [(\hat{x}^b_{t+1})_i - \bar{\hat{x}}^b_{t+1}][(\hat{x}^b_{t+1})_i - \bar{\hat{x}}^b_{t+1}]^T + Q_{t+1}, \tag{11}$$

$$(P_{\hat{y},\hat{y}})_{t+1} = \sum_i^{2L} w_i^{(c)} [(\hat{y}_{t+1})_i - \bar{\hat{y}}_{t+1}][(\hat{y}_{t+1})_i - \bar{\hat{y}}_{t+1}]^T + R_{t+1} \tag{12}$$

$$(P_{\hat{x}^b,\hat{y}})_{t+1} = \sum_i^{2L} w_i^{(c)} [(\hat{x}^b_{t+1})_i - \bar{\hat{x}}^b_{t+1}][(\hat{y}_{t+1})_i - \bar{\hat{y}}_{t+1}]^T \tag{13}$$

In the above equations, $w_i^{(c)}$ is the weight corresponding the *i*th sigma point (ensemble), $\sum_{i=0}^{2L} w_i^{(c)} = 1$, $Q = E(\eta_t \eta_t^T)$, and $R = E(\varepsilon_t \varepsilon_t^T)$.

2.3. Assimilation

$$(\hat{x}^a_{t+1})_i = (\hat{x}^b_{t+1})_i + K_{t+1}[y^o_{t+1} - (\hat{y}_{t+1})_i] \tag{14}$$

$$K_{t+1} = P_{\hat{x}^b,\hat{y}} {P_{\hat{y},\hat{y}}}^{-1} \tag{15}$$

$$(P^a_x)_{t+1} = (P_{\hat{x}^b,\hat{x}^b})_{t+1} - K_{t+1} P_{\hat{y},\hat{y}} K^T_{t+1} \tag{16}$$

In the above equations, y^o_{t+1} is the perturbed observation.

$$c = \sqrt{L+\lambda}$$

$$w_0^{(m)} = \frac{\lambda}{L+\lambda}$$

$$w_0^{(c)} = \frac{\lambda}{(L+\lambda)} + 1 - \alpha^2 + \beta$$

$$w_i^{(m)} = w_i^{(c)} = \frac{1}{2(L+\lambda)}, \qquad i = 1, 2, \ldots, 2L$$

$$\lambda = \alpha^2 (L+\kappa) - L$$

In the above equations, λ is a scaling parameter with a value that has a direct effect on the scaling of the sigma points. When $\lambda > 0$ the sigma points are scaled further from the mean, $\overline{X^a_t}$ [*Julier et al.*, 2000, 2002; *Julier and Uhlmann*, 2004]. The parameter α determines the spread of the sigma points around the mean state, $\overline{X^a_t}$, and is set to a small positive value, $(0 \leq \propto \leq 1)$. The parameter $k \geq 0$ guarantees positive definiteness of the covariance matrix and its default value is 0; β is a nonnegative weighting term that can be used to include higher-order behavior of the system states. If the prior distribution is Gaussian, B = 2 is optimal

[*Julier*, 2002; *Van der Merwe et al*., 2004]. Based on the settings of the values in the literature and some sensitivity experiments, we chose the values of $\alpha = 1$; $k = 0$; and $\beta = 2$ in this study.

The above algorithm also reveals that the weight of each ensemble member in calculating the error statistics could be different in the SPKF method, which differs from EnKF because the weight of each ensemble member is identical with EnKF.

3. Efficient Sigma-Point Kalman Filter

3.1. Singular Value Decomposition (TSVD) for SPKF (T-TSVD Scheme)

In the SPKF approach, there are 2L + 1 sigma points (ensemble members), where L is the dimension of the augmented state vector *X*. Usually, L is very large for realistic atmospheric or oceanic models, which is computationally unaffordable. A solution is to use the truncated principal component analysis (TPCA) or singular value decomposition (TSVD) to reduce the number of sigma points [*Ambadan and Tang*, 2009; *Luo and Moroz*, 2009]. Because the covariance matrix is symmetric, the solution could be expressed as follows:

$$P^a_{X,t} = E^a_{X,t} \Sigma_t (E^a_{X,t})^T \tag{17}$$

where $\sum_t = diag(\sigma^1_t, \sigma^2_t, \ldots, \sigma^L_t)$ is a diagonal matrix of eigenvalues that are sorted in descending order (i.e., $\sigma^1_t \geq \sigma^2_t \geq \cdots \geq \sigma^L_t$) and

$$E^a_{X,t} = (e^a_{X,t,1}, e^a_{X,t,2}, \ldots, e^a_{X,t,L}) \tag{18}$$

where $e^a_{X,t,i}$ is the *i*th eigenvector of $P^a_{X,t}$. Truncating the first *m* modes, the sigma points (4) can be written as follows:

$$\begin{aligned} \chi^k_0 &= \bar{X}^a_t; \\ \chi^+_{i,t} &= \bar{X}^a_t + c\sqrt{\sigma^i_t} e^a_{X,t,i} \\ \chi^-_{i,t} &= \bar{X}^a_t - c\sqrt{\sigma^i_t} e^a_{X,t,i} \end{aligned} \tag{19}$$

where $i = 1, 2 \ldots m$. Thus, the ensemble size becomes 2 * *m* + 1. Fast SVD algorithms such as Lanczos and block Lanczos [*Golub and van Loan*, 1996, chapter 9] can be used here. The application of the truncated SVD was also applied in *Ehrendorfer and Tribbia* [1997] when addressing high-dimensional systems.

3.2. Efficient TSVD-SPKF (ET-SPKF Scheme)

The TSVD scheme for SPKF proposed above can effectively release computational burden by truncating the analysis error covariance P^a_X to reduce sigma points. However, for a high-dimensional system, the P^a_X is often a very large matrix that will most likely require more memory than current computer systems can provide, Therefore, it is difficult or even impossible to apply the T-SPKF scheme to realistic high-dimensional atmospheric and oceanic models. To address this challenge, we propose a new scheme that uses a small matrix to generate sigma points by equations (18) and (19), which is implemented by using the relationship of eigenvectors between two relevant matrices [e.g., *von Stoch and Zwiers*, 2001] described as follows:

[1] Similar to equation (6), a covariance matrix is calculated in ensemble space, which is the matrix M0 by M0 instead of the P^0_X of L by L:

$$(\tilde{P}^a_{X,t}) = (X^a_t)^{tr} * (X^a_t).$$

[2] Calculate the eigenvector $\tilde{e}^a_{X,t}$ of $\tilde{P}^a_{X,t}$. This step serves the calculations of $e^a_{X,t}$ of $P^a_{X,t}$, which are required to construct the sigma points (ensemble members) by equations (18) and (19). The eigenvectors and eigenvalues of $(\tilde{P}^a_{X,t})$ are denoted by $\tilde{E}^a_{X,t}$ and Λ, where $\Lambda_t = diag(\lambda^1_t, \lambda^2_t, \ldots, \lambda^L_t)$ and $\tilde{E}^a_{X,t} = (\tilde{e}^a_{X,t,1}, \tilde{e}^a_{X,t,2}, \ldots, \tilde{e}^a_{X,t,L})$. The eigenvalue and eigenvector equations are as follows [*von Stoch and Zwiers*, 2004]:

$$(\tilde{P}^a_{X,t})\tilde{E}^a_{X,t}=\tilde{E}^a_{X,t}\Lambda_t$$
$$(X^a_t)^{tr} * X_t{}^a\tilde{E}^a_{X,t}=\tilde{E}^a_{X,t}\Lambda_t \quad (20)$$

Multiplying by X^a_t on the both sides of equation (20), we arrive at the following:

$$P^a_{X,t} * X_t{}^a\tilde{E}^a_{X,t}=X_t{}^a\tilde{E}^a_{X,t}\Lambda_t \quad (21)$$

Comparing equation (21) with equation (17) reveals the relationship between $\tilde{E}^a_{X,t}$ and $E^a_{X,t}$:

$$E^a_{X,t}=X_t{}^a\tilde{E}^a_{X,t}$$
$$\Lambda_t=\Sigma_t \quad (22)$$

Furthermore, normalization is performed for the *j*th eigenvector from equation (22) to ensure a unified norm:

$$e^a_{X,t,j}=X_t{}^a\tilde{e}^a_{X,t,j}/|X^a_t\tilde{e}_{X,t,j}| \quad (23)$$

where |.| is the L-2 norm. If the first m lead modes are truncated, then equations (23), (18), and (19) produce $2m+1$ important sigma points (i.e., $2m+1$ ensemble members) from which we can calculate error statistics and assimilate observations using equations (14–16).

[3] $\tilde{P}^a_{X,t}$ is then calculated from the $2m+1$ ensemble members, and its eigenvector is calculated using equation (23) and keeping the first m modes to generate $2m+1$ sigma points and ensemble members for assimilation and statistical analysis. Step (2) is repeated until the assimilation ends.

4. ET-SPKF Applied to the Lorenz Model

In this section, we explore the feasibility of using the ET-SPKF algorithm as an effective data assimilation method for highly nonlinear models. The Lorenz 1996 [*Lorenz*, 2006] model is generally used for this purpose. In the field of data assimilation, this model, accompanying with the Lorenz 3-component (1963) model, is often served as a test bed for examining the properties of various data assimilation schemes [e.g., *Miller et al*., 1994; *Abandan and Tang*, 2009; *Kalnay et al*., 2012] because it is not only computationally efficient, allowing various experiments, but also includes many dynamic features of realistic weather systems [e.g., *Lorenz*, 2006]. For example, it has error growth characteristics similar to those of full NWP (Numerical Weather Models).

The model contains variables $x_1,\ldots,x_i,\ldots,x_{Nx}$, which can be considered as atmospheric variables in Nx sectors of a latitude circle, governed by the following:

$$\frac{dx_i}{dt}=-x_{i-1}(x_{i-2}-x_{i+1})-x_i+F \quad (24)$$

where $i=1, 2,\ldots, Nx$ and the cyclic boundary conditions are $x_0=x_{Nx}$, $x_{-1}=x_{Nx-1}$, $x_{Nx+1}=x_1$. F is a forcing constant. It is assumed that the unit of time $\Delta t=1$ is associated with 5 days. A more detailed discussion of the model and its characteristics can be found in *Lorenz* [2006] and *Lorenz and Emmanuel* [1998].

The experimental setup is similar to that of *Lorenz* [2006], where $Nx=40$ and the magnitude of the forcing is set to eight, in which the system is chaotic. The true data are created by integrating the system over 4000 time steps by using the fourth-order Runge-Kutta scheme with a specified initial condition (denoted by $\mathbf{X}_0$). The integration step is set to 0.05 (i.e., 6 h). The observation data sets are generated by adding normally distributed noise $N(0,\sqrt{2})$ to the true data.

The assimilation experiment was carried out by adding normally distributed noise $N(0,\sqrt{2})$ to the specified initial condition $\mathbf{X}_0$. To implement the SPKF method, the state vector is redefined as the concatenation of the model states, model errors, and measurement errors as discussed in section 2.1. For a full-rank sigma-

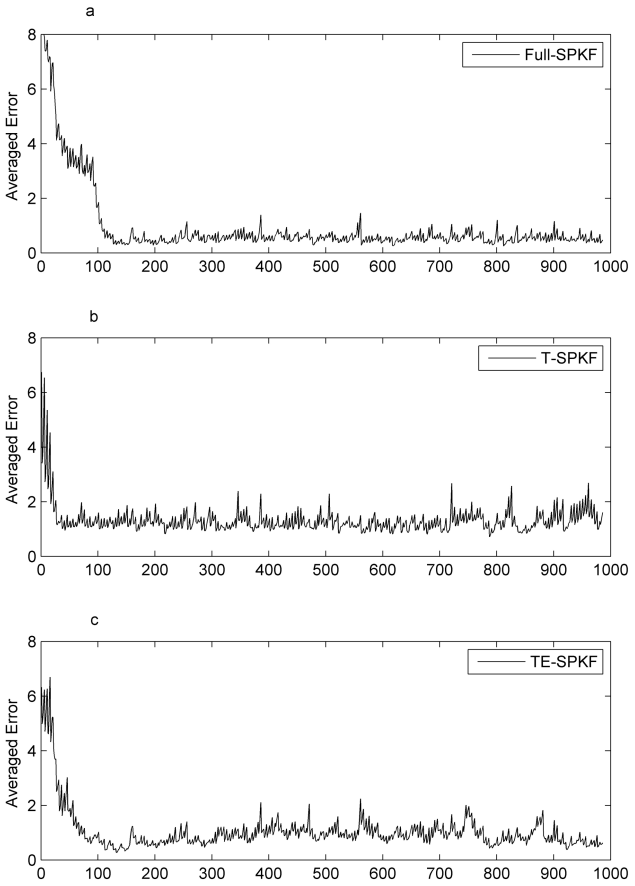

Figure 1. The variation of the averaged error (AE) over the 40 variables with time step for (a) full-rank SPKF, (b) T-SPKF with 31 sigma points (ensemble members), and (c) TE-SPKF with 31 sigma points. The AE is defined by the root error square of analysis against the true value (see context).

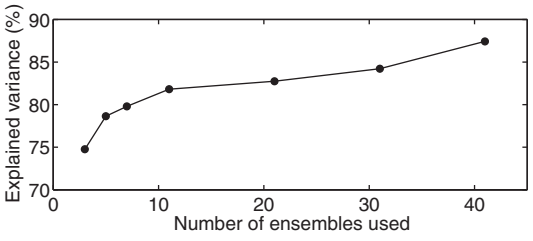

Figure 2. The variance explained by the truncated mode (ensembles) with respect to the total variance for ET-SPKF scheme. The total variance is $\tilde{P}_x^a$.

point space, we have a total of 241 sigma-points (2L + 1 = 2 * 120 + 1), or 241 ensemble members. We assume that the model and observation errors are uncorrelated in both space and time and that the observations of all model states are available and assimilated every five time steps. Because there is no general method of setting the model error, the magnitude of model error used in the Kalman filter is often determined experimentally by trial and error or by statistical methods such as the Monte Carlo [*Miller et al*., 1994] method. In our experiments, the model errors were intentionally designed in such a way that the model would not drift too far from the true state (The model is considered to have a relatively large error at initiation, so the assimilation weighs more observation information. As such, the model prediction would not drift too far from the true value). The model errors (Q) are incorporated into the assimilation by equation (11).

Figure 1a shows the variation of the averaged error (AE) over the 40 variables with time step t for the full-rank SPKF, where the AE is defined by the mean of the root error square of analysis x_t^a against x_t overall variables:

$$AE_t = \frac{1}{40}\sum_{i=1}^{40}\left(x_{i,t}^a - x_{i,t}\right)^2, \quad i = 1, 2, \ldots, 40$$

where i is the index of model variables. SPKF can result in a very small AE for the estimation of the model states after approximately 120 steps of assimilation. In the second case, we used the T-SPKF to reduce sigma points. In this case, we selected 31 sigma points that account for more than 83% of the total variance, as indicated in Figure 2. The result of this experiment is shown in Figure 1b. The model states can be fairly well estimated by the reduced T-SPKF, although its AE is not as small as the full SPKF. In the third case, the ET-SPKF algorithm is used to reduce sigma points. As in the second case, we chose 31 sigma points. Shown in Figure 1c is the AE of the state estimate from the ET-SPKF algorithm. A comparison between Figures 1c and 1b reveals that the reduced ET-SPKF is comparable with the T-SPKF with the same approximate error magnitude, suggesting a possible solution to applying SPKF in high-dimensional systems.

Similar to T-SPKF, one important element in the ET-SPKF scheme is the size of the truncated modes of TSVD, or effective sigma points. A small size fails to characterize important error statistics and leads to poor assimilation analyses, whereas a large size is likely computationally unaffordable. In the T-SPKF approach, a

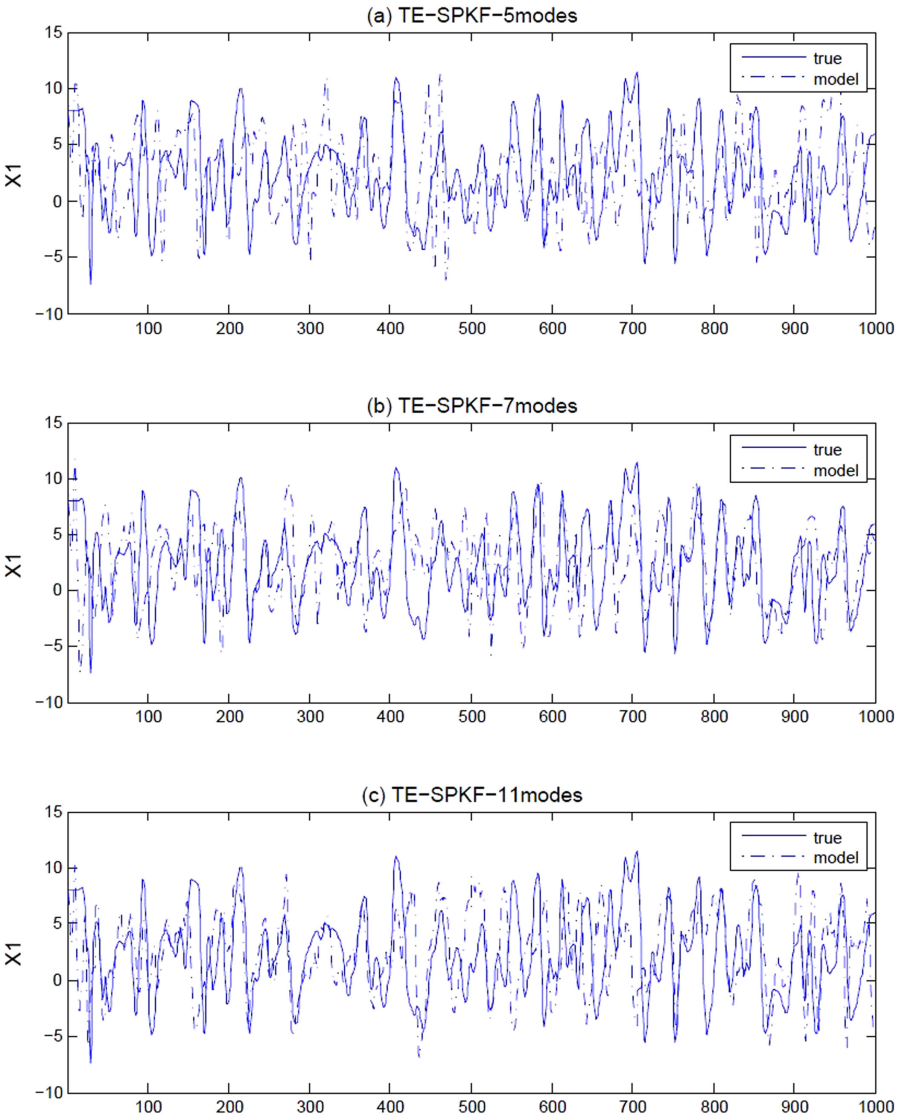

Figure 3. Comparison between the true value and analysis of ET-SPKF. The analysis from the truncated modes of 5, 7, and 11 are shown in Figures 3a–3c, indicating a poor analysis below 11 modes.

good strategy for determining the size of the truncated modes is based on the variance explained by the truncated modes with respect to the total variance of a full-rank covariance matrix P_x^a. However, for ET-SPKF, the total variance P_x^a is unknown because ET-SPKF only calculates the covariance $\tilde{P}_x^a$ of the ensemble space, which is related to the number of initial perturbations. Therefore, one challenge in using ET-SPKF is determining the truncated modes. An approximate solution is to explore the explained variance with respect to the total variance of $\tilde{P}_x^a$, as shown in Figure 2. As shown in this figure, the variance explained increases of ensemble size, but the rate is not much higher, especially beyond the size of 11. However, as shown in Figure 3, the assimilation experiment with 11 ensemble members is poor, indicating that such a strategy may not be useful.

Another strategy for the determination of the truncated modes is the sensitivity experiment, which is often used in EnKF and examines the analysis error as a function of the ensemble size. Figure 4 displays the variation of the AE with time step for different truncated modes (i.e., ensemble size). As shown in Figure 4, when the number of sigma points increases from 21 to 31, the average error quickly decreases, whereas when the numbers of sigma points changes from 31 to 41, the improvement in the analysis is not very significant. This suggests that 31 sigma points are most likely sufficient to characterize the error statistics in this case.

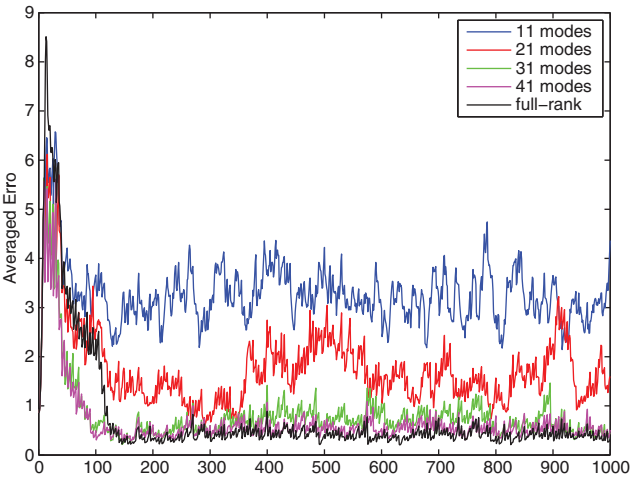

Figure 4. The variation of the averaged error (AE) over the 40 variables with time step for the different truncated modes (i.e., ensemble size) for the ET-SPKF scheme.

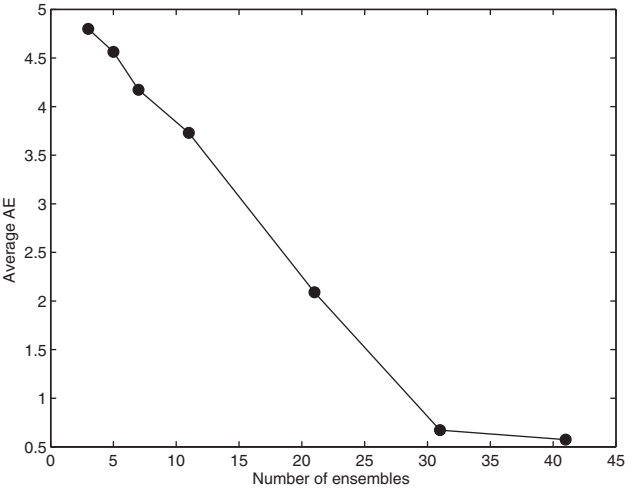

Figure 5. The mean of the average error over the entire assimilation period as a function of the truncated modes (ensemble size) for the ET-SPKF scheme.

Figure 5 shows the mean of the AE over the entire assimilation period as a function of ensemble size, further confirming that the ensemble size of 31 is sufficient and that the improvement with additional points is only subtle.

5. Application of the ET-SPKF Algorithm in the Ocean General Circulation Model

In this section, we apply the ET-SPKF algorithm into a realistic oceanic model. Emphasis here is placed on exploring the possibility of using ET-SPKF to assimilate multiple-oceanic data into a high-dimensional oceanic general circulation model (OGCM). Until now, the application of SPKF for the earth sciences has been confined to highly simplified, low-dimensional dynamical systems, such as the Lorenz model [*Ambadan and Tang*, 2009; *Luo and Moroz*, 2009].

5.1. The Ocean General Circulation Model (OGCM)

The model used herein is the oceanic component of the model Nucleus for European Modeling of the Ocean (NEMO) version (2.3) with free surface, which has been widely used for oceanic modeling and analysis [e.g., *Thomson et al*., 2006; *Thomson and Liu*, 2009; *Zhu and Demirov*, 2011]. Both the global and regional models that have the same spatial and temporal resolution are used in this study. The former is used for climatology runs and the latter is used for control runs and assimilation runs. The regional model domain used in this study is the Pacific Ocean between 60°N and 60°S and between 116°E and 66°W, for a total of 90 × 95 horizontal grid points. The horizontal resolution in the zonal direction is 2°, whereas the resolution in the meridional direction is 0.5° within 5° of the equator, smoothly changing up to 2.0° at 30°N and 30°S and then changing down to 1.0° at 60°N and 60°S. There are 31 unevenly spaced levels along the vertical profile with 24 levels concentrated in the upper 2000 m. The thickness of the levels varies from 10 m at the surface (within the first 105 m) to 500 m below the 3000 m level. The maximum depth is set to 5000 m, and a realistic topography based on the ETOPO5 (Earth Topography 5 min) global atlas is used [*Ferry et al*., 2007]. The NCEP (National Center for Environmental Prediction) reanalysis wind stress [*Behringer et al*., 1998] (http://www.esrl.noaa.gov/psd/), monthly climatological heat and freshwater fluxes [*Esbensen and Kushnir*, 1981] are used to force the model. During the integration, the heat fluxQ_s is adjusted by the following:

$$Q_s = Q_0 + \lambda(T - T_0)$$

where Q_0 is the climatological heat flux [*Esbensen and Kushnir*, 1981], T is the model SST, T_0 is Levitus' observed climatological SST [*Levitus*, 1998], and λ is the relaxation rate set to $-40\ \mathrm{Wm^{-2}K^{-1}}$. For a 50 m, mixed-layer depth, this value corresponds to a relaxation time scale of 2 months [*Madec et al*., 2008].

The model has biases in the temperature and salinity simulations compared to the observed climatology [*Deng et al*., 2010]. To reduce these biases online, the spectral nudging method proposed by *Thompson et al*. [2006] is used in this study and is based on the method in *Deng et al*. [2012] and *Keppenne et al*. [2008].

The model is forced for 200 years with the NCEP monthly climatological mean wind stress, which is derived from the 50 year NCEP reanalysis wind stress and the heat flux Q_s to arrive at an initial state. From this initial condition, the model is forced by the actual monthly NCEP wind stress to simulate conditions for the period 1981–2004. The ocean state at the end of 2004 provided the initial condition for the control run that started on 1 January 2005. The control run for the period 2005–2007, forced by NCEP reanalysis wind stress without data assimilation, provides a basis for comparison.

5.2. Data

The data used for assimilation in this study is the best-copy temperature and salinity profiles from the GTSPP (Global Temperature and Salinity Profile Program) Continuously Managed Database (http://www.nodc.noaa.gov/GTSPP/access_data/gtspp-bc.html), which covers the Pacific Ocean for 2005–2007. The best-copy data (hereafter BCD**)** assembled profiles for Argo, expendable bathythermograph (XBT), conductivity-temperature-depth (CTD), Tropical Atmosphere-Ocean (TAO)/Triangle Trans-Ocean Buoy Network (TRITON) provided the most complete data sets without duplication. Only the profiles that are flagged "good" are chosen for assimilation. The other data set for assimilation is the low-resolution ($1^\circ \times 1^\circ$, Mercator grid) gridded satellite sea level anomaly (SLA) from the (M)SLA and (M)ADT (Absolute Dynamic Topography) near-real times and delayed time products [e.g., *Deng et al*., 2012], which is a homogeneous, intercalibrated and highly accurate long-time series of SLA altimeter data downloaded from the website (http://www.aviso.oceanobs.com). Because the resolution of the SLA data is much higher than the model resolution in most of the model domains, a thinning scheme is used to reduce the assimilation of SLA data. Thus, only one SLA observation in a four-grid box is assimilated. The data sets used for validation include the Ocean Surface Current Analyses (real time) (http://www.oscar.noaa.gov), withheld SLA observations and withheld T-S profiles. The surface current is derived from satellite altimeter and vector wind data; details can be found in *Bonjean et al*. [2002] and *Helber et al*. [2007].

5.3. ET-SPKF Assimilation System

In oceanic data assimilation, there are still many important issues that must be addressed when developing a realistic assimilation system by the ensemble-based methods, e.g., the observation and random model error, the efficiency of computation, and the initial perturbation. This section primarily tests the algorithm of the ET-SPKF method rather than develop an optimal assimilation system. For simplicity, we will directly apply the parameters used in the EnKF assimilation system developed by *Deng et al*. [2012]. It should be noted that the parameters used in *Deng et al*. [2012] were based on their own sensitivity experiments; therefore, they may not be optimal for the ET-SPKF approach, and the results presented here are a conservative performance of the ET-SPKF algorithm. Below is a brief introduction to these parameter settings. A detailed discussion about these parameters can be found in *Deng et al*. [2011, 2012].

5.3.1. Observation Error

Argo profiles and other observations are used in this study. To solve the problem of redundant observation, a subdata set is constructed by the "data thinning" approach prior to each assimilation step to ensure that there is only one observation within a model grid cell and assimilation window (of 11 days, see below). Priority is given to Argo profiles in the construction of the subdata set due to its importance in this study. Such a data thinning approach is not optimal in the data assimilation context because information may be lost in some analyses. However, it can effectively reduce the cost of computation.

Argo floats have a 10 day resampling period; thus, available Argo profiles are sparse on any specific day. To solve the temporal sparsity of Argo data, we treat all Argo data within a time window of 11 days as the observations used for the assimilation [e.g., *Oke et al*., 2008; *Deng et al*., 2012]. In this study, the assimilation interval is 5 days. Thus, the 11 day window is much longer than the assimilation interval, which ensures sufficient observations at a single assimilation step. This 11 day time window is centered at the day of analysis. Thus, the observations for the day of the analysis and the observations for 5 days before and after the analysis day are used at each assimilation step. In this time window, all Argo profiles within a model grid cell are sorted according to the differences between the time of analysis and that of the

observations. The profile that has the minimum time difference is finally used in the assimilation. If no Argo observations are available in this process, other data sets are explored using the same scheme as for the Argo profiles.

Observation error includes measurement errors and representation errors. Usually, it is assumed to be uncorrelated between locations; thus, its covariance matrix is diagonal, obtained by the observation error of all data within the 11 day time window. In this study, the observation perturbation is drawn from the Gaussian distribution, with the mean equal to zero and the variance equal to the error square, according to the method of *Deng et al*. [2012].

5.3.2. Model Error

In this study, random model error is introduced into the assimilation using equation (11), where Q is the model error covariance, which is equivalent to random model errors introduced by adding noise to the forecast ensemble at the analysis time (without integrating noise in the model). For simplicity, we also assumed the model error to be uncorrelated between locations; thus, its covariance matrix is diagonal.

The magnitude of Q_t is determined using a fraction of the root mean square error (RMSE). For temperature, salinity and SLA, the RMSE is estimated by comparing the observations of the time delayed Argo T-S profiles and SLA against the output of control run over the period of 2002–2004. For simplicity, we only consider the vertical variations of the perturbation amplitudes. We calculate RMSE for each model level using all paired observation-model data for the period 2002–2004 and average the standard deviations over the horizontal model domain to produce their vertical profiles. After many sensitivity experiments with different combinations of the perturbation amplitudes, we set the amplitude to 10% of the RMSE for temperature and salinity at each vertical level and 0.013 m for SLA (10% of SLA RMSE). These settings are somewhat artificial but were adjusted by sensitivity experiments to reach an accurate assimilation performance for the EnKF experiment developed in *Deng et al*. [2012].

5.3.3. Local Analysis

To address computational efficiency and the spurious correlation between distant locations in the background covariance matrix, localization is often used in EnKF [e.g., *Gaspari and Cohn*, 1999; *Houtekamer and Mitchell*, 2001; *Oke et al*., 2005; *Hunt et al*., 2007; *Oke et al*., 2008; *Deng et al*., 2010] to assimilate all observations that may affect the analysis at a given grid point simultaneously and obtain the analysis independently for each model grid point. However, as stated in the introduction, sigma points in SPKF are derived based on a global analysis error covariance matrix and the localizations cannot be used for generating sigma points. Unfortunately, global analysis without localization causes two issues for a high-dimensional system: (1) updating the state analysis using equations (14) and (15) is expensive; (2) the spurious correlation of distant locations degrades the analysis. Therefore, we propose a hybrid approach that globally generates sigma points (ensemble members) and locally analyzes the model states. After the analysis of each grid for the entire domain is obtained locally by equations (14) and (15), the ET-SPKF algorithm is used to generate globally derived sigma points that are propagated by Equation (7), resulting in a recursive algorithm until the assimilation ends. The covariance localization function used here is defined as $\rho(x,y,z)=e^{-\left\{\left(\frac{dx}{Lx}\right)^2+\left(\frac{dy}{Ly}\right)^2+\left(\frac{dz}{Lz}\right)^2\right\}}$, where dx, dy, and dz are the distances between the analysis grid and its surrounding grids in the zonal, meridional, and vertical, respectively. The localization length scales are set to Lx = 3000 km $\times$ cos(θ), Ly = 1500 km $\times$ cos(θ), and Lz = 100 m in the three directions, according to the sensitivity experiments, where θ is the latitude at the analysis grid.

After all grids over the model domain are analyzed, a final analysis ensemble can be obtained. The box used in localization smoothly shifts with the analysis grid. With the local analysis strategy, this size is most likely sufficient in estimating the error covariance matrix. A detailed discussion on the localization scheme used in this study can be found in *Deng et al*. [2012].

5.4. Results

For evaluation of the assimilation performance by ET-SPKF, we first calculate the RMSE of temperature and salinity of the assimilation run and control run without assimilation against the observed BCD profiles. The RMSE is defined as follows:

$$RMSE = \sqrt{\frac{1}{NL}\sum_{k=1}^{L}\sum_{i=1}^{N}\left(Y_{i,k}^{m} - Y_{i,k}^{o}\right)^2},$$

where Y is the variable of evaluation, the superscript "o" denotes the observations and "m" denotes the model (prediction), N is the number of total observations within the domain of evaluation, and L is the number of total assimilation steps over the 3 years from 2005 to 2007.

Considering the sparse distribution of in situ observations, we used a 5 day window, centered on the analysis time to calculate RMSE, and all observations falling in this window are used in calculating RMSE. The RMSE is calculated for each bin of 5° (lon.) × 5° (lat.) from 30°S–55°N to 120°E–80°W to ensure that sufficient observations were used.

The mean temperature and salinity RMSEs, averaged over model levels in the top 250 m, from the control run and assimilation run are shown in Figures 6a and 6c and in Figures 6b and 6d, respectively. As shown in Figure 6a, the temperature in the control run indicates two large RMSE areas located in the Kuroshio area and the central and eastern equatorial Pacific. There are also two relatively small RMSE areas located in the north-east Pacific and the south-east tropical Pacific region. Figure 6c shows that the large RMSE values of salinity in the top 250 m occur in a belt between the equator and 15°S and areas near the Kuroshio region.

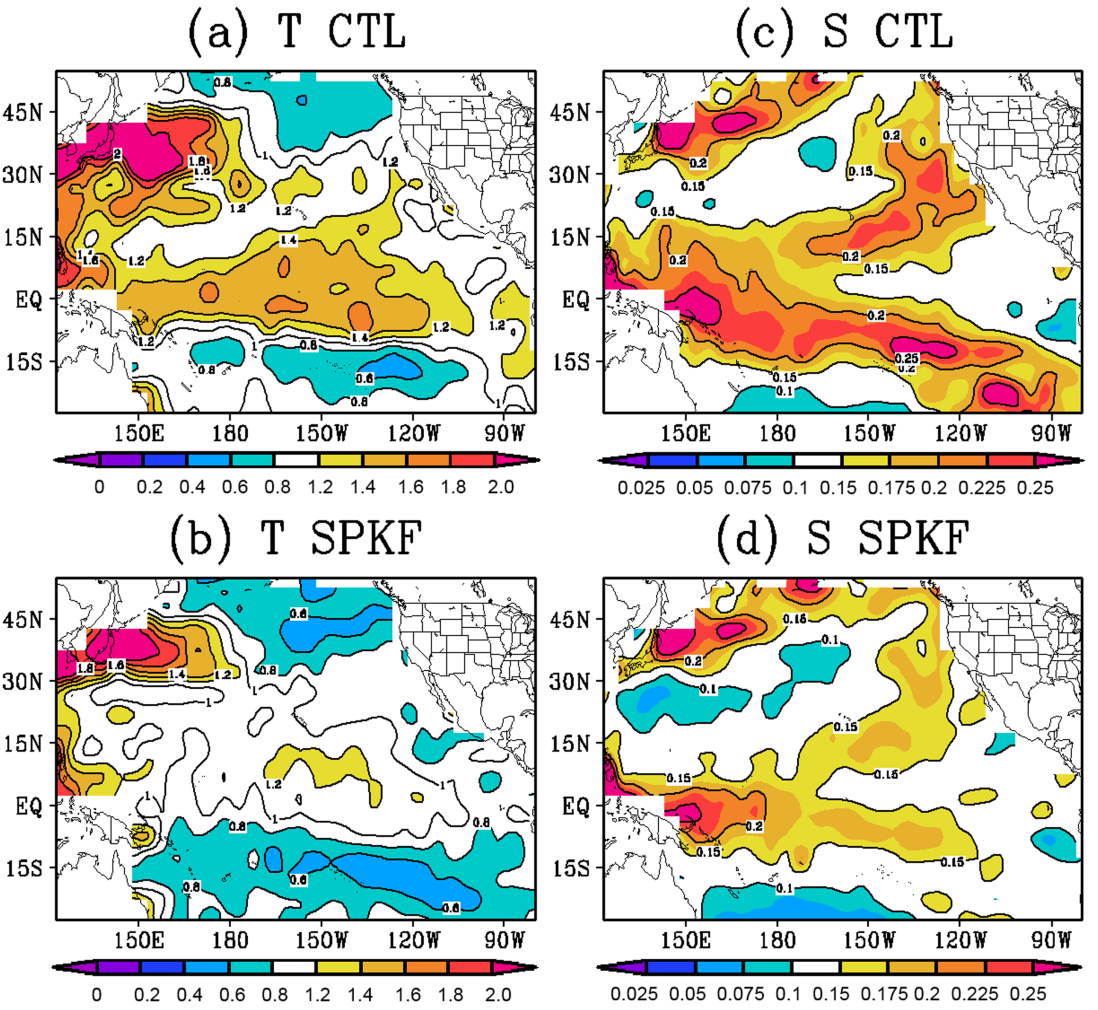

Figure 6. The mean RMSEs of (a and b) temperature and (c and d) salinity averaged over model levels in the top 250 m from the control run and assimilation run for 3 years (2005–2007) and where the observations are the BCD profiles. The contour interval is 0.2°C for temperature and 0.05 psu (practical salinity unit) for salinity.

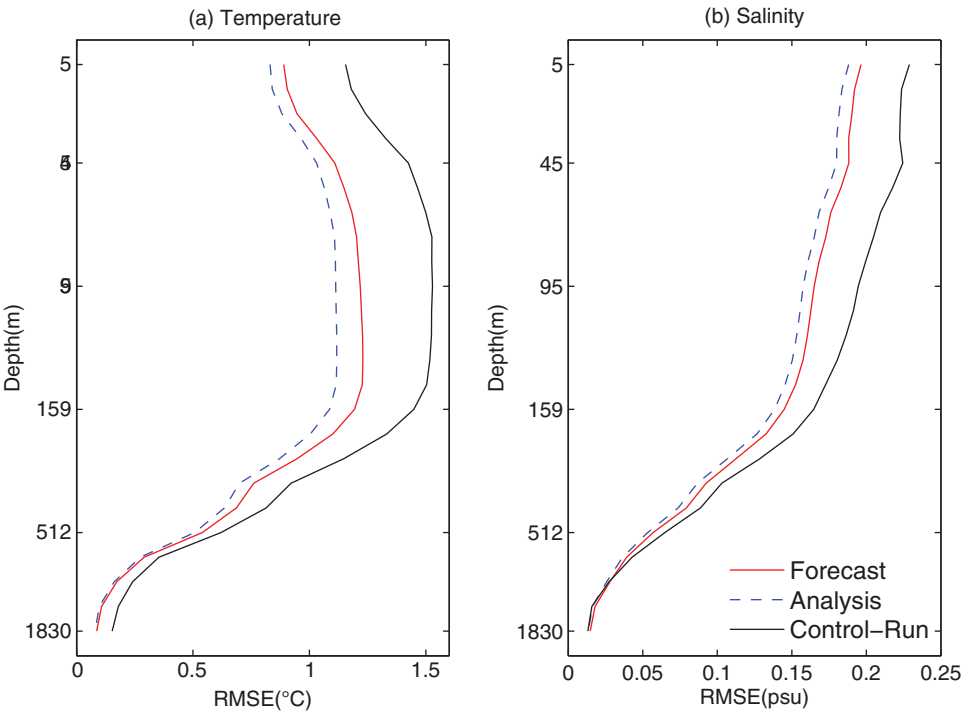

Figure 7. The mean RMSEs of (a) temperature and (b) salinity averaged over the domain of 30°S–55°N and 120°E–80°W as a function of depth from the control experiment (black line), the prediction (red thin line), and analysis (dotted blue line).

Apparently, there are always large errors in both temperature and salinity in the Kuroshio region, implying the difficulty in simulating the ocean state of that region because of strong currents.

Comparing the control run (Figure 6a) with the assimilation run (Figure 6b) reveals that the RMSEs of temperature are significantly reduced by assimilation, especially in the central and eastern equatorial Pacific. Similarly, with the data assimilation, the amplitudes of the salinity RMSE, shown in Figure 6d, are also significantly reduced. The above results demonstrate that the ET-SPKF assimilation scheme can improve the oceanic temperature and salinity simulations over the entire Pacific Ocean. It should be noted, however, that over some subregions, such as the Kuroshio regions, there are still relatively large RMSE values that are not thoroughly removed by the data assimilation. The possible causes for these large RMSE values are the insufficiency of observation, coarse model spatial resolution, improper expression of the forecast error and complicated dynamics that the ocean model does not resolve.

The overall impacts of the assimilation on the reduction of the prediction and analysis RMSE can be demonstrated by the vertical RMSE profiles of temperature and salinity averaged over the whole assimilation region for 3 years, as shown in Figure 7. Compared to the control run, the assimilation significantly reduces the temperature and salinity RMSE of the upper ocean at 500 m, in particular for the temperature simulation. This is more visible in Figure 8, which shows the temporal evolution of RMSE of each time step at the depths of 50 and 150 m. As shown, the assimilation significantly reduces the temperature and salinity RMSEs at all time steps at both depths. Apparently, the improvement of the assimilation is more significant for temperature than for salinity and for the near-surface (50 m) than for the subsurface (150 m), which is most likely because temperature has a greater variability than salinity and the deeper ocean is less varied. These results further confirm that this ET-SPKF scheme is capable of improving the simulations of oceanic state and is applicable for constructing realistic assimilation systems.

A further validation of the ET-SPKF assimilation is performed by exploring its impact on hindcast skill. A hybrid-coupled model is applied to perform the El Niño–Southern Oscillation (ENSO) hindcast experiment, which is a prediction experiment for a previous time period. This hybrid model is composed of the OGCM and a linear atmospheric model, as reported in *Deng et al.* [2008]. Starting from the initial conditions provided by the ET-SPKF assimilation run and control run, 33 hindcast experiments are conducted for the

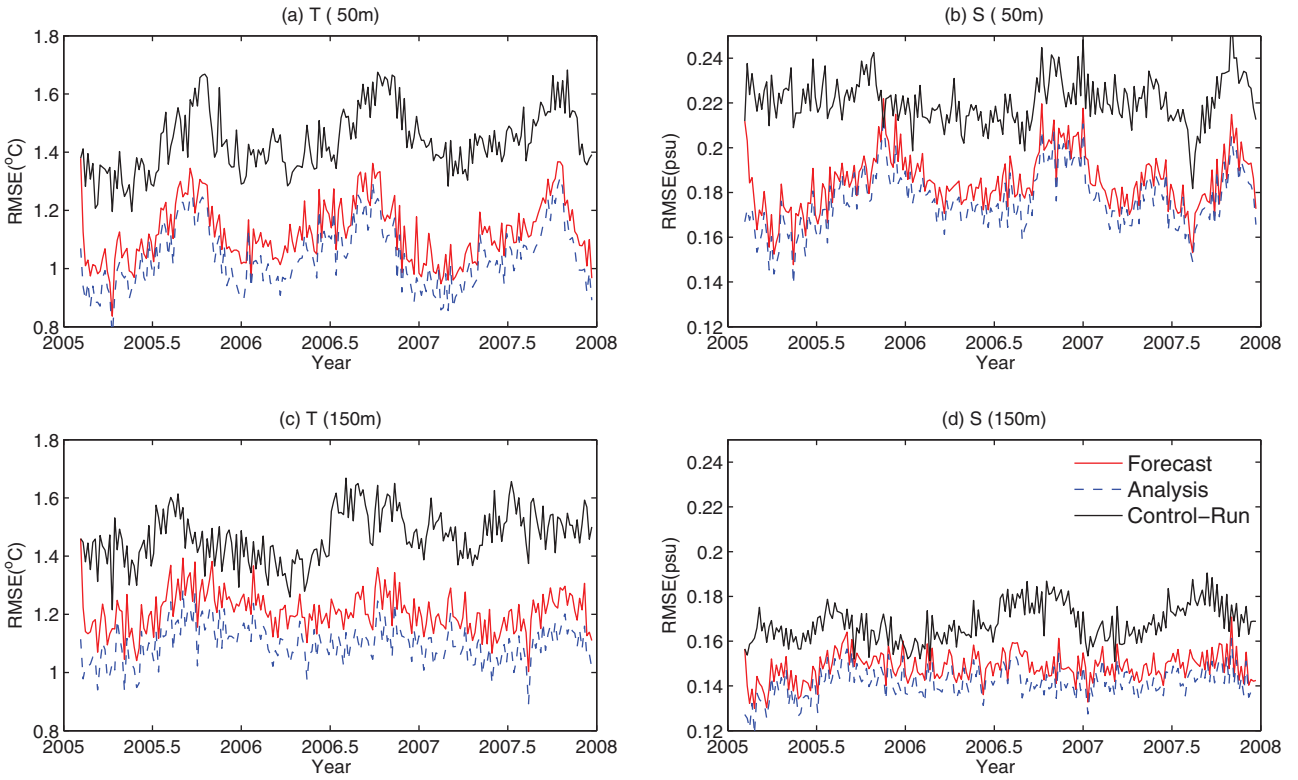

Figure 8. The mean RMSE of (a and c) temperature and (b and d) salinity over the domain of 30°S–55°N and 120°E–80°W at the depth of 50 and 150 m and derived from the control run without assimilation (black), prediction (red), and analysis (blue) of ET-SPKF.

period from April 2005 to December 2007. Figure 9 shows the hybrid coupled model's predictive skills initialized from the control run and the assimilation, where the predicted El Niño 3.4 (5°S–5°N, 120°W–170°W) SSTA index is compared against the observed values. As shown, the predictions from both the assimilation and the control run beat persistence from the second month. Compared with the control run, the assimilation produces a remarkable improvement in correlations for all lead times and RMSE skill in the first 9 months. It is not clear why the assimilation does not produce improvements in the RMSE for lead time beyond 9 months, but the ET-SPKF assimilation system is capable of improving the ENSO hindcast skill, especially for the correlation skill.

6. Summary and Discussion

In the current framework of the EnKF algorithm, the ensemble members were generated randomly by perturbing model states with a subtle difference. The ensemble size required to estimate the accuracy of error variance was unknown because the true error covariance was always unknown. This hinders the design of the assimilation system to a certain extent, although it is generally considered that additional ensemble members increase the accuracy. Alternatively, a deterministic method has been used to generate ensemble members for the SPKF approach, which precisely estimates the error covariance. However, the SPKF method requires a large ensemble size and is computationally unfeasible for high-dimensional systems. Recently, effort has been made toward the development of reduced rank SPKFs that significantly decrease the number of sigma points (ensemble members). This approach is usually implemented by using TSVD or TPCA to produce sigma points with leading modes. However, the reduced rank methods are based on an explicit expression of the prediction error covariance matrix, which creates a huge challenge because of its computational costs and memory storage demands when analyzing high-dimensional systems.

In this work, we propose a new strategy, ET-SPKF, to calculate the lead modes of TSVD for reduced rank SPKFs. ET-SPKF calculates the analysis error covariance matrix on ensemble space. The formation of SVD leading modes between the raw data space and the ensemble space is then introduced, which allows the ET-SPKF algorithm to calculate the sigma points without directly evaluating the analysis error covariance

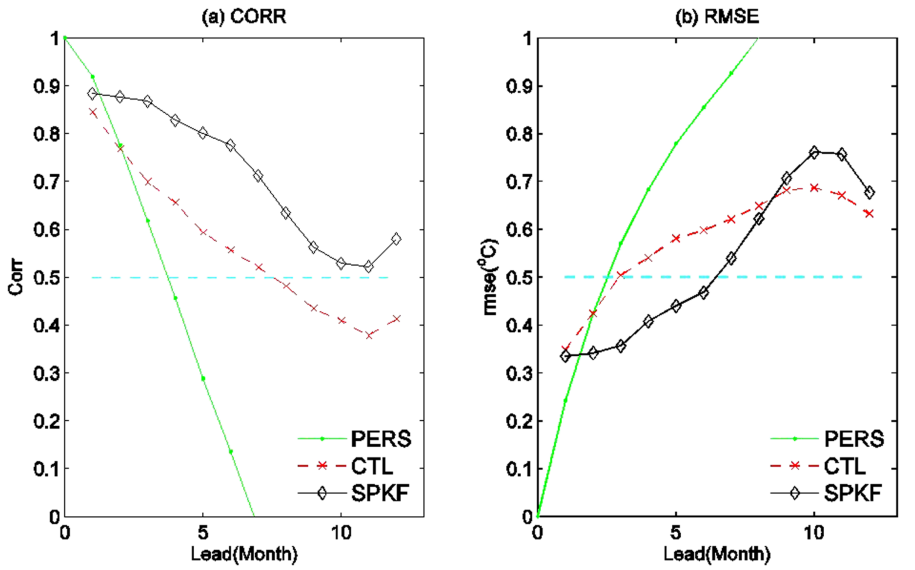

Figure 9. (a) The correlation and (b) RMSE between observed and predicted SST anomalies in the El Niño event in the 3.4 region as a function of lead time. The predictions are initialized every month from April 2005 to December 2007. The dark line is from the prediction initialized from the control run, and the red line is from the prediction initialized from the ET-SPKF assimilation. The persistent skill is also presented (green line).

matrix of model state space globally. Further, while the sigma point is generated globally, the analysis of model states and Kalman gain are performed according to a localization scheme, making the ET-SPKF approach computationally efficient for high-dimensional systems.

The ET-SPKF approach is first tested using a 40-variable Lorenz model and then extended to a realistic oceanic general circulation model. The results show that the scheme, which makes use of a hybrid strategy for high-dimensional systems, i.e., global sigma points and local analysis, is capable of producing good model-state analyses. In particular, for the realistic oceanic assimilation case, the ET-SPKF assimilation can significantly improve oceanic analysis and the ENSO prediction skill.

One interesting issue is how the ET-SPKF approach performs when compared to the conventional EnKF algorithm. Figures 10a and 10b are the same as Figures 6b and 6d; however, Figures 10a and 10b were derived by the EnKF algorithm, whereas Figures 6b and 6d were derived by the ET-SPKF algorithm. Both algorithms used the same settings in all prescribed parameters, including the model error, observation error, decorrelation scale and ensemble size. Figures 10c and 10d show the difference between the two methods (Figures 10a and 10b minus Figures 6b and 6d). As shown in Figures 10c and 10d, the ET-SPKF algorithm is comparable to the EnKF algorithm in most regions of the assimilation domain for temperature and salinity, except in the equatorial region, where the ET-SPKF algorithm is better than the EnKF algorithm for temperature. In the west-northern Pacific region, the EnKF algorithm is more accurate than the ET-SPKF algorithm. However, caution should be used in interpreting the comparisons because the performance of these assimilations may be sensitive to the prescribed settings. When one parameter is optimal for one assimilation method, it may not be suitable for another method, and vice versa. Thus, it is challenging, and perhaps impossible, to conduct a fair comparison between these assimilation methods. For example, the prescribed settings used in EnKF and ET-SPKF, as shown in Figures 6 and 10, are based on our earlier work of EnKF using numerous sensitivity experiments. These settings may not be optimal for ET-SPKF. Namely, if well-defined parameters can be obtained for ET-SPKF, a more accurate performance than what is shown in Figures 10a and 10b can be expected. However, our objective is not to compare ET-SPKF and EnKF. Alternatively, we focus on the development of a computationally efficient algorithm for SPKF, making the SPKF approach that has been widely used in machine learning, engineering and statistical modeling applicable in the earth sciences. A great deal of additional research is required before a fair comparison between ET-SPKF and EnKF can be made. Nevertheless, the results reported in this work are promising, and a variety of possible extensions to the SPKF approach could be developed to address more complicated situations.

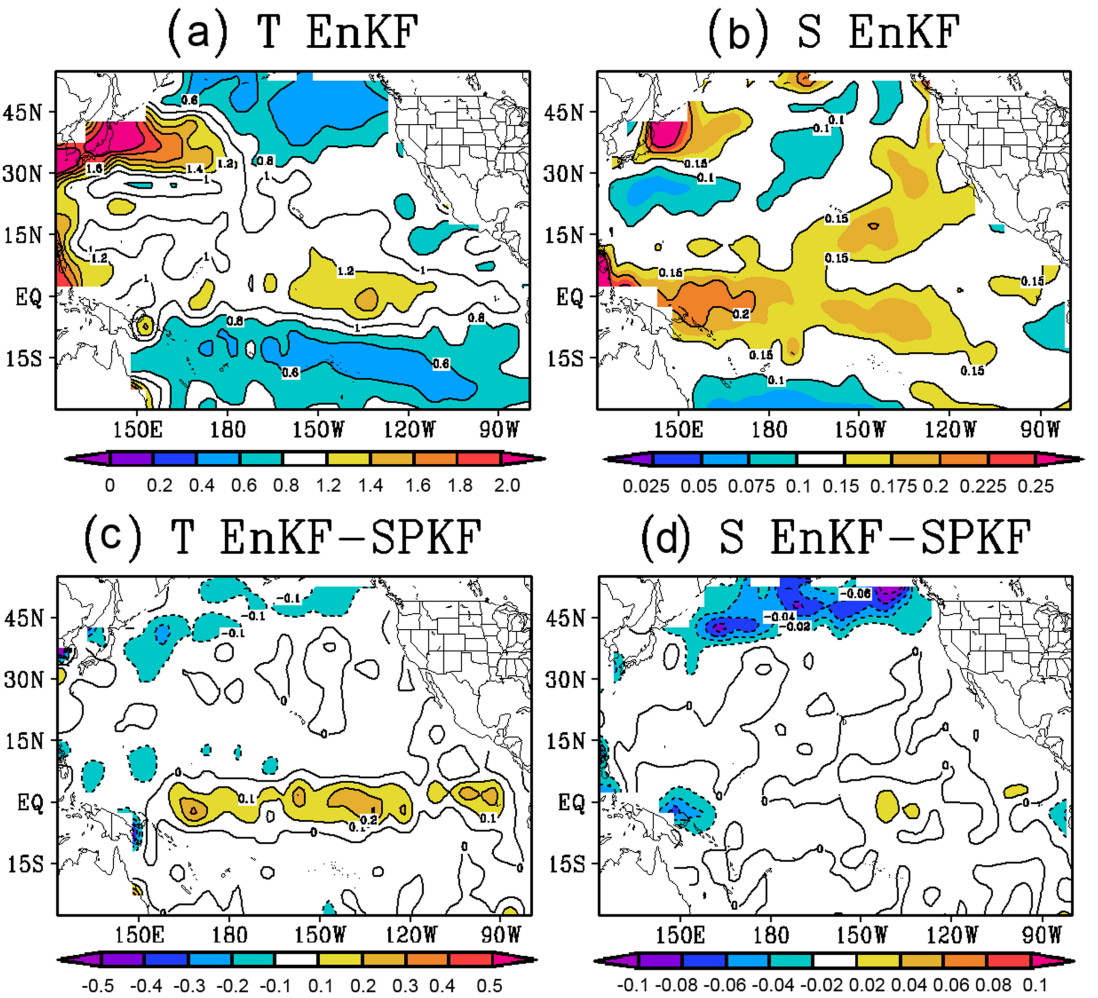

Figure 10. (a and b) Same as Figures 6a and 6c but use the EnKF method for assimilation; (c and d) the differences in the RMSE between the two methods in which negative values indicate that the EnKF method is more accurate than the ET-SPKF method and vice versa.

Acknowledgments
This work is supported by the National Science Foundation of China (41276029) and the NSERC (Natural Sciences and Engineering Research Council of Canada) Discovery grant.

References

Ambadan, T. J., and Y. Tang (2009), Sigma-point Kalman filter data assimilation methods for strongly nonlinear systems, *J. Atmos. Sci.*, *66*(2), 261–285.

Behringer, D. W., M. Ji, and A. Leetmaa (1998), An improved coupled model for ENSO prediction and implications for ocean initialization. Part I: The ocean data assimilation system, *Mon. Weather Rev.*, *126*, 1013–1021.

Bonjean, F., and G. S. E. Lagerloef (2002), Diagnostic model and analysis of the surface currents in the tropical Pacific Ocean, *J. Phys. Oceanogr.*, *32*, 2938–2954.

Deng, Z., Y. Tang, and X. Zhou (2008), The retrospective prediction of ENSO from 1881–2000 by a hybrid coupled model—(I): SST assimilation with ensemble Kalman filter, *Clim. Dyn. 32*:(2-3), 397–413.

Deng, Z., Y. Tang, and G. Wang (2010), Assimilation of Argo temperature and salinity profiles using a bias-aware localized EnKF system for the Pacific Ocean, *Ocean Modell.*, *25*, 187–205.

Deng, Z., Y. Tang, and H. J. Freeland (2011), Evaluation of several model error schemes in the EnKF assimilation: Applied to Argo profiles in the Pacific Ocean, *J. Geophys. Res.*, *116*, C09027, doi:10.1029/2011JC006942.

Deng, Z., Y. Tang, D. Chen, and G. Wang (2012), A hybrid ensemble generation method for EnKF for Argo data assimilation, *Atmos. Ocean*, *50*, 129–145.

Ehrendorfer, M., and J. Tribbia (1997), Optimal prediction of forecast error covariances through singular vectors, *J. Atmos. Sci.*, *54*, 286–313.

Esbensen, S. K., and Y. Kushnir (1981), The heat budget of the global ocean: An atlas based on estimates from surface marine observations, *Rep. 29*, 244 pp., Clim. Res. Inst., Oregon State Univ., Corvallis, Oreg.

Evensen, G. (2003), The ensemble Kalman filter: Theoretical formulation and practical implementation, *Ocean Dyn.*, *53*, 343–367.

Fan, C., and Z. You (2009), Highly efficient sigma points filter for spacecraft attitude and rate estimation, *Math. Prob. Eng.*, 2009, 1–23.

Ferry, N., E. Rémy, P. Brasseur, and C. Maes (2007), The Mercator global ocean operational analysis system: Assessment and validation of an 11-year reanalysis, *J. Mar. Syst.*, *65*, 540–560, doi:10.1016/j.jmarsys.2005.08.004.

Gaspari, G., and S. E. Cohn (1999), Construction of correlation functions in two and three dimensions, *Q. J. R. Meteorol. Soc.*, *125*, 723–757.

Golub, G., and C. van Loan (1996), *Matrix Computations*, 3rd ed., Johns Hopkins Univ. Press, London.

Helber, R. W., R. H. Weisberg, F. Bonjean, E. S. Johnson, and G. S. E. Lagerloef (2007), Satellite-derived surface current divergence in relation to tropical Atlantic SST and wind, *J. Phys. Oceanogr.*, *37*, 1357–1375.

Houtekamer, P., and H. Mitchell (2001), A sequential ensemble Kalman filter for atmospheric data assimilation, *Mon. Weather Rev.*, *129*, 123–137.

Hunt, B., E. Kostelich, and I. Szunyogh (2007), Efficient data assimilation for spatiotemporal chaos: A local ensemble transform Kalman filter, *Physica D*, *230*, 112–126.

Julier, S., J. Uhlmann, and H. F. Durrant-Whyte (2000), A new method for the nonlinear transformation of means and covariances in filters and estimators, *IEEE Trans. Autom. Control*, *45*(3), 477–482.

Julier, S. J. (2002), The scaled unscented transformation, American Control Conference, 2002. Proceeding of the 2002, IEEE, vol. *6*, pp. 4555–4559.

Julier, S. J., and J. K. Uhlmann (2002), Reduced sigma point filters for the propagation of means and covariances through nonlinear transformation, in *2002 Proceedings of American Control Conference*, pp. 887–892, IEEE Press, Anchorage, Ak.

Julier, S. J., and J. K. Uhlmann (2004), Unscented filtering and nonlinear estimation, *Proc. IEEE*, *92*(3), 401–422.

Julier, S. J., J. K. Uhlmann, and H. F. Durrant-Whyte (1995), A new approach for filtering nonlinear systems, In The Proceedings of the American Control Conference, IEEE, pp. 1628–1632, Seattle WA, USA.

Kalnay, E., Y. Ota, T. Miyoshi, and J. Liu (2012), A simpler formulation of forecast sensitivity to observations: Application to ensemble Kalman filters, *Tellus, Ser. A*, *64*, 18462, doi:10.3402/tellusa.v64i0.18462.

Keppenne, C. L., M. M. Rienecker, J. P. Jacob, and R. Kovach (2008), Error covariance modeling in the GMAO ocean ensemble Kalman filter, *Mon. Weather Rev.*, *136*, 2964–2982.

Levitus, S., and T. Boyer (1998), *NODC (Levitus) World Ocean Atlas 1998*, Phys. Sci. Div., Earth Syst. Res. Lab., Boulder, Colo. [Available at http://www.esrl.noaa.gov/psd/data/gridded/data.nodc.woa98.html.].

Lorenz, E. N. (1963), Deterministic non-periodic flow, *J. Atmos. Sci.*, *20*, 130–141.

Lorenz, E. N. (2006), Predictability-A problem partly solved, in *Predictability of Weather and Climate*, edited by T. Palmer and R. Hagedorn, pp. 40–58, Cambridge Univ. Press, New York.

Lorenz, E. N., and K. A. Emanuel (1998), Optimal sites for supplementary weather observations: Simulations with a small model, *J. Atmos. Sci.*, *55*, 399–414.

Luo, X., and I. M. Moroz (2009), Ensemble Kalman filter with the unscented transform, *Physica D*, *238*, 549–562.

Madec, G. (2008), *"NEMO Ocean Engine". Note du Pole de Modélisation*, vol. *27*, Inst. Pierre-Simon Laplace, France.

Miller, R. N., M. Ghil, and F. Gauthiez (1994), Advanced data assimilation in strongly nonlinear dynamical systems, *J. Atmos. Sci.*, *51*, 1037–1056.

Morelande, M. R., and B. Ristic (2006), Reduced sigma point filtering for partially linear models, acoustics, speech and signal processing, paper presented at ICASSP 2006 Proceedings. 2006 IEEE International Conference, Toulouse, France, 14–19 May.

Oke, P. R., A. Schiller, D. A. Griffin, and G. B. Brassington (2005), Ensemble data assimilation for an eddy-resolving ocean model of the Australian Region, *Q. J. R. Meteorol. Soc.*, *131*, 3301–3311.

Oke, P. R., G. B. Brassington, D. A. Griffin, and A. Schiller (2008), The Bluelink Ocean Data Assimilation System (BODAS), *Ocean Modell.*, *21*, 46–70.

Thompson, K. R., D. G. Wright, Y. Lu, and E. Demirov (2006), A simple method for reducing seasonal bias and drift in eddy resolving ocean models, *Ocean Modell.*, *13*, 109–125.

Tippett, M. K., J. L. Anderson, C. H. Bishop, T. M. Hamill, and J. S. Whitaker (2003), Ensemble square root filters, *Mon. Weather Rev.*, *131*, 1485–1490.

Van der Merwe, R., and E. A. Wan (2001), The square-root unscented Kalman filter for state and parameter estimation, paper presented at the International Conference on Acoustics, Speech, and Signal Processing (ICASSP), IEEE, Salt Lake City, Utah.

Van der Merwe, R., E. A. Wan, and S. I. Julier (2004), Sigma-point Kalman filters for nonlinear estimation and sensor fusion: Applications to integrated navigation, in AIAA Guidance, Navigation and Control Conference, pp. 5120–5122, Am. Inst. of Aeronaut. and Astronaut., Providence, R. I.

von Storch, H., and F. W. Zwiers (2001), *Statistical Analysis in Climate Research*, pp. 484, Cambridge. Univ, Cambridge, UK.

Wan, E. A., and R. van der Merwe (2001), The unscented Kalman filter, in *Kalman Filtering and Neural Networks*, edited by S. Haykin, chap. *7*, 62 pp., John Wiley, New York.

Zhu, J., and E. Demirov (2011), On the mechanism of interannual variability of the Irminger Water in the Labrador Sea, *J. Geophys. Res.*, *116*, C03014, doi:10.1029/2009JC005677.

Zupanski, M. (2005), Maximum likelihood ensemble filter: Theoretical aspects, *Mon. Weather Rev.*, *133*, 1710–1726.